First-order Raman spectra and lattice dynamics of a $NdGaO_3$ crystal

J. Suda*
Department of Electronic Engineering, Aomori Polytechnic College, Goshogawara 037-0002, Japan

T. Mori
Department of Electrical Engineering, Ibaraki National College of Technology, Fukayatsu, Nakane, Katsuta, Ibaraki 312-0011, Japan

H. Saito†
Department of Material Science and Technology, Faculty of Science and Technology, Hirosaki University, Hirosaki 036-8561, Japan

O. Kamishima and T. Hattori
Institute of Multidisciplinary Research for Advanced Materials, Tohoku University, Katahira, Aoba-ku, Sendai 980-8577, Japan

T. Sato
Department of Material Science and Technology, Faculty of Science and Technology, Hirosaki University, Hirosaki 036-8561, Japan
(Received 2 July 2001; revised manuscript received 7 June 2002; published 6 November 2002)

The phonon-dispersion curves of the $NdGaO_3$ crystal are calculated on the basis of a rigid-ion model by using the measured frequency values by Raman and infrared polarized spectroscopy at room temperature. The temperature dependence of the molar heat capacity of $NdGaO_3$ is also calculated using the one-phonon density of states obtained from the phonon-dispersion curves. The first-order polarized Raman spectra of the A_{1g} mode in the $NdGaO_3$ crystal have been measured in the temperature range between 31 and 500 K. The temperature dependence for the linewidth of the A_{1g} modes has been analyzed at 339 and 470 cm^{-1} by using the phonon-dispersion curves, and the calculated result reproduces the observed one in the temperature range 31–500 K. Thus, the temperature dependence of the linewidth of the A_{1g} modes in the $NdGaO_3$ crystal is approximately explained by the cubic anharmonic term in the expansion series of the crystal potential energy.

DOI: 10.1103/PhysRevB.66.174302 PACS number(s): 78.30.−j, 63.90.+t

I. INTRODUCTION

Phonon-dispersion curves are very important for studying lattice dynamics, because atomic interactions, specific heat, elastic constants, dielectric constants, and other physical properties are derived from phonon-dispersion curves. However, as seen in the book by Bilz and Kress,[1] phonon-dispersion curves were calculated for relatively simple crystals. Recently, the temperature dependence of Raman-active phonon spectra in SnO_2, TeO_2, and GeO_2 crystals have been studied by Sato and Asari,[2] Kimura and Sato,[3] and Sato and Suda,[4] respectively. Furthermore, using lattice-dynamical perturbative treatment, we have also observed anharmonic effects in phonon spectra in the case of aragonite-type,[5,6] calcite-type,[7] and sheelite-type[8–10] crystals having complicated structures. We found that the quartic anharmonic term of the first-order perturbation, as well as the cubic term of the second-order one, and thermal expansion contribute to the temperature dependence of the frequency shift of external Raman-active phonon modes in sheelite-type crystals.[9,10] Up to now, no clear tendency has been found in the contribution of the cubic and quartic anharmonic terms to the linewidth.

Optical applications (such as microwave filters) of high-T_c superconducting films require the knowledge of the infrared properties of substrates, since the penetration depth of radiation is often comparable to or greater than the film thickness.[11–13] The optical properties of MgO and $SrTiO_3$, which are widely used as substrates for depositing high-T_c superconducting materials, have been investigated by several research groups.[14–17] Recently, ferroelectric thin films (e.g., $PbTiO_3$) or high-T_c superconducting films (e.g., $YBa_2Cu_3O_7$) were also grown epitaxially on other materials, such as $LaAlO_3$, $LaGaO_3$, and $NdGaO_3$, with the small lattice misfits and the small difference of thermal-expansion coefficients with these thin films, and small dielectric constants in the microwave-frequency region.[18–23] The $NdGaO_3$ crystal belongs to the orthorhombic system [space group $Pbmn(D_{2h}^{16})$] (Ref. 20) with lattice constants $a=0.5426$, $b=0.5496$, and $c=0.7707$ nm. It is composed of twenty atoms per unit cell with a highly complicated crystal structure. The optical active phonon spectra and complex dielectric function of $NdGaO_3$ have been studied by several researchers.[24–28] The temperature dependence of the Raman peaks for $LaGaO_3$ and $NdGaO_3$ has been measured by Sanjuan *et al.*[28] from 300 to 860 K. They found for the $NdGaO_3$ crystals that the usual slight softening of the mode frequencies is accompanied by line broadening as the temperature increases, but this crystal has no phase transition below 1816 K.[28] To our knowledge, phonon-dispersion curves of $NdGaO_3$ have not been reported until now. Also, the origin of the temperature dependence of the phonon spectra of $NdGaO_3$ is not understood yet by not only phonon dispersion but also the quantitative calculation of the anharmonic theory.

Therefore, our purpose is to determine the phonon-dispersion curves for a relatively complicated $NdGaO_3$ crystal. In the calculation of the phonon-dispersion curves of the $NdGaO_3$ crystal, a conventional rigid-ion model is em-

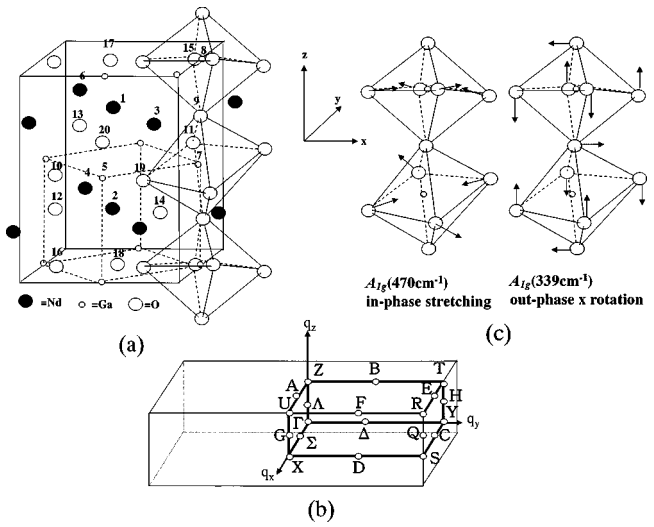

FIG. 1. (a) Orthorhombic unit cell, (b) first Brillouin zone (in which thick solid lines represent irreducible Brillouin zone) for D_{2h}^{16} materials, and (c) A_{1g} phonon modes at 339 and 470 cm^{-1}.

ployed, where the potential coefficients have been determined by a least-squares fitting of the calculated frequencies at the Γ point to the experimental ones measured by Raman and infrared (IR) polarized spectroscopy at room temperature. In addition, the observed temperature dependence of the linewidth of Raman-active phonons is examined by the lattice-dynamical calculation for phonon-dispersion curves.

II. EXPERIMENT

The unit cell of $NdGaO_3$ contains 20 atoms and the labeled atoms by Wychoff notation[29,30] are shown in Fig. 1(a). The fractional coordinates for each atom are given in Table I. The $NdGaO_3$ crystal belongs to an orthorhombic system [space group $D_{2h}^{16}(Pbnm)$] (Ref. 20) and it is a distorted perovskite system. The specimen used in the present study was a transparent single crystal with a greenish brown tinge and its purity was better than 99.995% (prepared by Fit Company, Ltd). It was cut perpendicularly to the *a*, *b*, and *c* axes [$7\times6\times8$ (*c* axis) mm^3 in dimension], respectively, and its surface was optically polished. In order to determine these phonon frequencies at room temperature, we measured the polarized Raman spectra in a right-angle geometry and the polarized infrared reflected spectra for three principal directions.

Polarized Raman-scattering spectra of the A_{1g} modes were measured from 31 to 500 K in the right-angle scattering geometry. The excitation source was the 488.0-Å line of an Ar^+-ion laser at a power level of 100–200 mW. The scat-

TABLE I. Fractional coordinates and coordinates of atomic positions and cell dimensions (Å).

Atomic number[a]	Atom[a]	Fractional coordinates[b]			Coordinates		
		ξ	η	ζ	x	y	z
1	Nd	−0.0180	0.0060	0.2500	−0.0977	0.3298	1.9268
2	Nd	0.0180	−0.0060	−0.2500	0.0977	−0.3298	−1.9268
3	Nd	0.5180	0.5600	0.2500	2.8107	3.0778	1.9268
4	Nd	−0.5180	−0.5600	−0.2500	−2.8107	−3.0778	−1.9268
5	Ga	0.5000	0.0000	0.0000	2.7130	0.0000	0.0000
6	Ga	0.5000	0.0000	0.5000	2.7130	0.0000	3.8535
7	Ga	0.0000	0.5000	0.0000	0.0000	2.7480	0.0000
8	Ga	0.0000	0.5000	0.5000	0.0000	2.7480	3.8535
9	O(1)	0.0500	0.4700	0.2500	0.2713	2.5831	1.9268
10	O(l)	−0.0500	−0.4700	−0.2500	−0.2713	−2.5831	−1.9268
11	O(1)	0.4500	0.9700	0.2500	2.4417	5.3311	1.9268
12	O(1)	−0.4500	−0.9700	−0.2500	−2.4417	−5.3311	−1.9268
13	O(2)	−0.2900	0.2750	0.0500	−1.5735	1.5114	0.3854
14	O(2)	0.2900	−0.2750	−0.0500	1.5735	−1.5114	−0.3854
15	O(2)	0.7900	0.7750	0.4500	4.2865	4.2594	3.4682
16	O(2)	−0.7900	−0.7750	−0.4500	−4.2865	−4.2594	−3.4682
17	O(2)	0.2900	−0.2750	0.5500	1.5735	−1.5114	4.2389
18	O(2)	−0.2900	0.2750	−0.5500	−1.5735	1.5114	−4.2389
19	O(2)	0.2100	0.2250	−0.0500	1.1395	1.2366	−0.3854
20	O(2)	−0.2100	−0.2250	0.0500	−1.1395	−1.2366	0.3854

Cell dimensions

a	*b*	*c*
5.426	5.496	7.707

[a]Atoms and atomic numbers correspond to the atomic positions in the unit cell shown in Fig. 1.
[b]From Ref. 30.

tered light was analyzed by a double monochromator (CT-1000D, Jasco Company) having the spectral resolution of about 2.0 cm^{-1}. The sample temperature was controlled with a closed-cycle He-gas cryostat (model U102 AW, Daikin Company). The wave number was calibrated with a plasma line of the Ar^+-ion tube. The accuracy of the wave number was ± 1 cm^{-1}.

Polarized infrared reflected spectra were measured in three principal directions. A Fourier-transform (FT) infrared spectrometer (IR-V1990, Jascoft) was employed to measure polarized infrared reflected spectra measured in three principal directions of (001), (010), and (100).

III. RESULTS AND DISCUSSION

The first Brillouin zone of $NdGaO_3$ is shown in Fig. 1(b). The phonons with the wave vector $\mathbf{q}=0$ are classified by the irreducible representation of the space group D_{2h}^{16} as follows:[20]

$$\Gamma = 7A_{1g} + 7B_{1g} + 5B_{2g} + 5B_{3g} + 8A_{1u} + 8B_{1u} + 10B_{2u} + 10B_{3u}.$$

Among them, the Raman- and the infrared-active modes are

$$7A_{1g} + 7B_{1g} + 5B_{2g} + 5B_{3g}$$

and

$$7B_{1u} + 9B_{2u} + 9B_{3u},$$

respectively, where the A_{1u} modes are optically silent and the remaining $1B_{1u}$, $1B_{2u}$, and $1B_{3u}$ modes correspond to three acoustic modes.

Figure 2 shows the polarization dependence of the observed Raman spectra at room temperature and 31 K. Below 100 cm^{-1}, a broad band is observed around 70 cm^{-1} in both the $Z(XZ)X$ and the $Z(YZ)X$ geometries, as shown in Figs. 2(a) and 2(b). The temperature dependence of their intensity is different from those of B_{2g} and B_{3g} modes in the same geometry. Thus, each broad band is not a first-order Raman spectrum, because this intensity is not proportional to a phonon occupation number.[31] We have assigned Raman-active lines as follows: seven A_{1g} modes (96, 145, 215, 290, 339, 414, and 470 cm^{-1}), four B_{1g} modes (153, 214, 363, and 449 cm^{-1}), four B_{2g} modes (144, 334, 405, and 463 cm^{-1}), and three B_{3g} modes (168, 199, and 351 cm^{-1}). These modes follow the phonon occupation number.[31] The present results are in good agreement with those observed by Sanjuan *et al.*[28]

In order to assign IR phonon center frequencies, we performed calculations of the infrared reflectance following the procedure described in Ref. 25 in the case of B_{1u}, B_{2u}, and B_{3u}, respectively. For example, Fig. 3 shows the comparison between our calculated reflectance and the observed one in the case of the B_{2u} mode. These values of center frequencies are approximately in good agreement with those observed by Zhang *et al.*[25] Thus, we obtained the final experimental phonon frequencies at the Γ point, as shown in Table II.

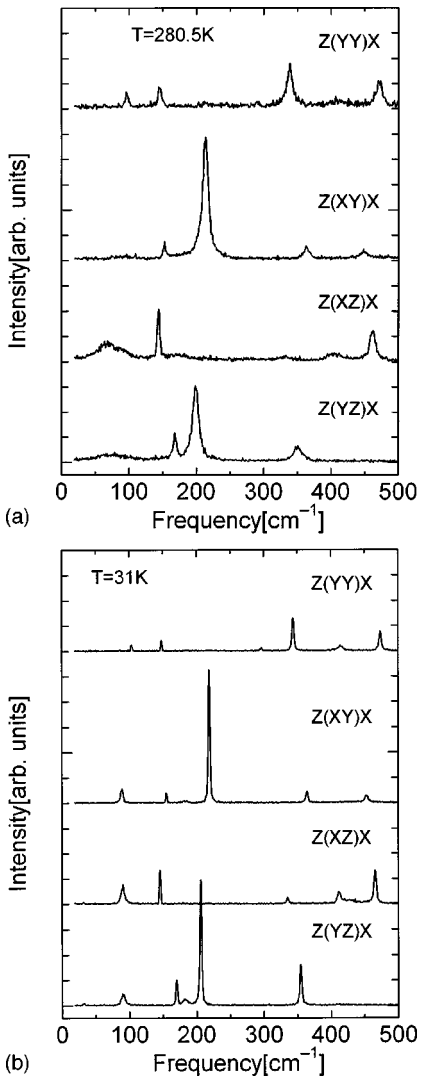

FIG. 2. Polarized Raman spectra at (a) 280.5 K; (b) 31 K.

The $NdGaO_3$ crystal exhibits both ionic and covalent features, owing to the covalent interactions inside the GaO_3^{-3} units and to the presence of Nd^{3+} ions. However, the experimental frequencies of optical-phonon (i.e., infrared and Raman) spectra of the $NdGaO_3$ crystal were smaller than 600 cm^{-1}. We calculated the phonon-dispersion curves of the $NdGaO_3$ crystal using the conventional rigid-ion model.[4] The rigid-ion model can be written as

$$m\omega^2\mathbf{U} = (H + zCz)\mathbf{U}, \tag{1a}$$

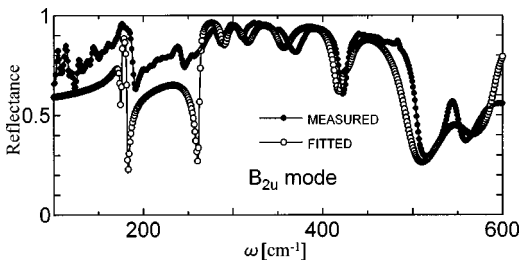

FIG. 3. Reflectance of $NdGaO_3$ at room temperature in the spectral region from 100 to 600 cm^{-1}.

TABLE II. Comparison between our calculated values of optical-phonon frequencies (cm^{-1}) and observed ones of $NdGaO_3$ using the conventional rigid-ion model.

Mode	Experimental values (cm^{-1})	Calculated values (cm^{-1})	Deviation values (cm^{-1})	Mode	Experimental values (cm^{-1})	Calculated values (cm^{-1})	Deviation values (cm^{-1})
A_{1g}	96.00	109.26	13.26	A_{1u}		337.02	
A_{1g}	145.00	150.88	5.88	A_{1u}		419.93	
A_{1g}	215.00	216.37	1.33	A_{1u}		505.30	
A_{1g}	290.00	298.41	8.41	B_{1u}	174.00	173.95	0.05
A_{1g}	339.00	355.04	16.04	B_{1u}		270.40	
A_{1g}	414.00	444.26	30.26	B_{1u}	290.00	299.20	9.20
A_{1g}	470.00	516.27	46.27	B_{1u}	300.00	314.58	14.58
B_{1g}		93.29		B_{1u}	321.00	355.99	34.99
B_{1g}	153.00	162.54	9.54	B_{1u}		430.31	
B_{1g}	214.00	215.94	1.94	B_{1u}	595.00	581.03	13.97
B_{1g}		316.25		B_{2u}		96.74	
B_{1g}	363.00	383.43	20.43	B_{2u}	174.00	174.42	0.42
B_{1g}	449.00	450.28	1.28	B_{2u}	260.00	251.58	8.42
B_{1g}		505.29		B_{2u}	290.00	283.33	6.67
B_{2g}	144.00	143.62	0.74	B_{2u}	321.00	304.51	16.49
B_{2g}		218.42		B_{2u}	356.00	338.52	17.48
B_{2g}	334.00	302.86	31.14	B_{2u}	424.00	415.78	8.22
B_{2g}	405.00	391.04	13.96	B_{2u}	545.00	477.84	67.16
B_{2g}	463.00	492.41	29.41	B_{2u}	595.00	552.97	42.03
B_{3g}	168.00	164.57	3.43	B_{3u}		134.42	
B_{3g}	199.00	197.63	1.37	B_{3u}	174.00	179.19	5.19
B_{3g}	351.00	346.91	4.09	B_{3u}	260.00	266.43	6.43
B_{3g}		418.01		B_{3u}	273.00	282.25	9.25
B_{3g}		504.68		B_{3u}	300.00	300.37	0.37
A_{1u}		136.71		B_{3u}	343.00	337.59	5.41
A_{1u}		171.92		B_{3u}	356.00	369.58	13.58
A_{1u}		228.89		B_{3u}		453.55	
A_{1u}		249.97		B_{3u}	595.00	537.99	57.01
A_{1u}		293.99					

where H is the matrix specifying the short-range atom-atom interaction, C is the Coulomb matrix for the long-range electrostatic interaction, m and z represent mass and ionic charge, respectively, and u denotes the displacement vector for atoms. The matrix C is calculated by Ewald's method. Here, the relationship between the repulsive matrix elements ($H_{\alpha\beta}$) and the repulsive crystal potentials ($\Phi^H_{\alpha\beta}$) is assumed to be[4]

$$\Phi^H_{\alpha\beta}(lk;l'k')=\begin{cases} -\left\{\dfrac{x_\alpha x_\beta}{r^2}\left[\phi''^H-\dfrac{1}{r}\phi'^H\right]+\dfrac{\delta_{\alpha\beta}}{r}\phi'^H\right\} \\ \qquad [(lk)\neq(l'k')], \\ \displaystyle\sum_{l'k}{}' \ \dfrac{x_\alpha x_\beta}{r^2}\left[\phi''^H-\dfrac{1}{r}\phi'^H\right]+\dfrac{\delta_{\alpha\beta}}{r}\phi'^H \\ \qquad [(lk)=(l'k')], \end{cases} \tag{1b}$$

where $\Phi^H_{\alpha\beta}(lk;l'k')$ is related to the atom-atom potential ϕ^H in the central approximation as follows:[4]

$$H_{\alpha\beta}(\mathbf{q}|kk')=\sum_{l'}{}' \ \Phi^H_{\alpha\beta}(lk;l'k')\exp[i\mathbf{q}\cdot\{\mathbf{x}(l'k')-\mathbf{x}(lk)\}]. \tag{2}$$

The prime on the sum Σ' indicates that the term of $lk=l'k'$ is omitted, and x_α and x_β represent the displacements of the Cartesian components α and β, respectively. We assumed the Born-Mayer-type function for $\phi^H(r_{ij})$ (representing the short-range potential) in Eqs. (1b), and also assumed that $\phi^H(r_{ij})$ is applied for all bonds having the bond length $r_{ij}\leqq 3.0$ Å, i.e., $j\leqq 22$, using the force constants given as[4]

$$A_j=\frac{V}{e^2}\left[\frac{\partial^2\phi^H(r_{ij})}{\partial r_i^2}\right]_0,$$

$$B_j=\frac{V}{e^2}\left[\frac{1}{r_i}\frac{\partial\phi^H(r_{ij})}{\partial r_i}\right]_0. \tag{3}$$

TABLE III. Parameters used to calculate the phonon-dispersion curves.

Potential		Parameter	Units			Bond type
Coulomb	ionic charge	Z_{Nd}	e	1.395		
		Z_{Ga}	e	1.094		
		$Z_{O(1)}$	e	−0.891		
		$Z_{O(2)}$	e	−0.799		
Repulsion	Force constant					
A_1	e^2/ν	121.0	B_1	e^2/ν	1.0	Ga-O(2)
A_2	e^2/ν	66.8	B_2	e^2/ν	−17.0	Ga-O(1)
A_3	e^2/ν	135.0	B_3	e^2/ν	−45.2	Ga-O(2)
A_4	e^2/ν	178.3	B_4	e^2/ν	1.0	Nd-O(1)
A_5	e^2/ν	305.0	B_5	e^2/ν	14.0	Nd-O(2)
A_6	e^2/ν	96.0	B_6	e^2/ν	87.0	Nd-O(2)
A_7	e^2/ν	1.2	B_7	e^2/ν	59.0	Nd-O(1)
A_8	e^2/ν	−32.0	B_8	e^2/ν	31.0	O(1)-O(2)
A_9	e^2/ν	37.0	B_9	e^2/ν	82.0	O(1)-O(2)
A_{10}	e^2/ν	27.0	B_{10}	e^2/ν	−19.0	Nd-O(2)
A_{11}	e^2/ν	−32.0	B_{11}	e^2/ν	1.0	O(2)-O(2)
A_{12}	e^2/ν	7.0	B_{12}	e^2/ν	−1.0	O(1)-O(2)
A_{13}	e^2/ν	−16.0	B_{13}	e^2/ν	11.0	O(2)-O(2)
A_{14}	e^2/ν	35.0	B_{14}	e^2/ν	−86.0	Nd-O(1)
A_{15}	e^2/ν	56.0	B_{15}	e^2/ν	6.0	O(1)-O(2)
A_{16}	e^2/ν	−24.0	B_{16}	e^2/ν	−18.0	O(2)-O(2)
A_{17}	e^2/ν	176.0	B_{17}	e^2/ν	61.0	Nd-Ga
A_{18}	e^2/ν	−90.0	B_{18}	e^2/ν	13.0	Nd-O(1)
A_{19}	e^2/ν	−22.0	B_{19}	e^2/ν	81.0	Nd-Ga
A_{20}	e^2/ν	16.0	B_{20}	e^2/ν	−9.0	Nd-O(2)
A_{21}	e^2/ν	82.0	B_{21}	e^2/ν	18.0	Nd-Ga
A_{22}	e^2/ν	−53.0	B_{22}	e^2/ν	−22.0	O(2)-O(2)

Here the derivatives of the short-range potential, A_j and B_j, represent the bond-stretching and the bond-bending force constants, respectively. The parameters used to calculate the phonon-dispersion curves are listed in Table III. The final phonon-dispersion curves are shown in Fig. 4(a). Our calculated frequencies at the Γ point are assigned to all phonon modes using the standard projection operator technique (as shown in Table IV) and are compared with experimental ones listed in Table II. The average deviation between calculated and experimental values at the Γ point is about 14.8 cm^{-1} (4.2%). The calculated frequencies are in good agreement for all modes with experimental ones except for three phonon peaks with high frequency, i.e., B_{2u} (545-), B_{2u} (595-), and B_{3u} (595-cm^{-1}) modes. These discrepancies most likely arise from some approximation (weakly distorted perovskite) of the rigid-ion model. However, taking into account the complexity of this class of material and rigid-ion model, we believe that the overall agreement between theory and experiment should be considered as reasonable.[43] As shown in Fig. 4(a), the phonon-dispersion curves are doubly degenerate on distinct points (i.e., *X, Y, Z, T*, and *R* points) of the irreducible Brillouin zone. These properties were expected as a result of the discussion based on group theory.[6]

The temperature dependence of the Raman linewidth is investigated using the present phonon-dispersion curves. The fundamental width of the lattice vibration in ionic crystals was calculated by Wallis, Ipatova, and Maradudin[32] using a Green's function. The cubic anharmonic term affects the linewidths more significantly than the quartic term in the temperature dependence of the first-order Raman spectra for the oxide crystals.[2–5,8,9] If the thermal-expansion coefficients have small values in several types of oxide crystals[2–5,8,9,37] with a high melting point and stable structure in the high-temperature region, the cubic anharmonic force coefficient[31–36] $|C_3|^2$ is independent of temperature. If the Raman linewidth $\Gamma_j^{(3)}(\omega)$ is caused only by the cubic anharmonic term in the crystal potential energy, the linewidth $\Gamma_j^{(3)}(\omega)$ is proportional to the two-phonon density of states with the factor $\pi\hbar\Omega|C_3|^2/(64N)$ as follows:[32]

$$\begin{aligned}\Gamma_j^{(3)}(\omega) \propto \sum_{q_1} \sum_{j_1,j_2} & \omega_{j_1}(\mathbf{q}_1)\omega_{j_2}(-\mathbf{q}_1)\{n_{j_1}(\mathbf{q}_1) \\ & + n_{j_2}(-\mathbf{q}_1)+1\}[\delta(\Omega-\omega_{j_1}(\mathbf{q}_1)-\omega_{j_2}(-\mathbf{q}_1)) \\ & - \delta(\Omega+\omega_{j_1}(\mathbf{q}_1)+\omega_{j_2}(-\mathbf{q}_1))]+[n_{j_1}(\mathbf{q}_1) \\ & - n_{j_2}(-\mathbf{q}_1)][\delta(\Omega+\omega_{j_1}(\mathbf{q}_1)-\omega_{j_2}(-\mathbf{q}_1)) \\ & - \delta(\Omega-\omega_{j_1}(\mathbf{q}_1)+\omega_{j_2}(-\mathbf{q}_1))], \qquad (4)\end{aligned}$$

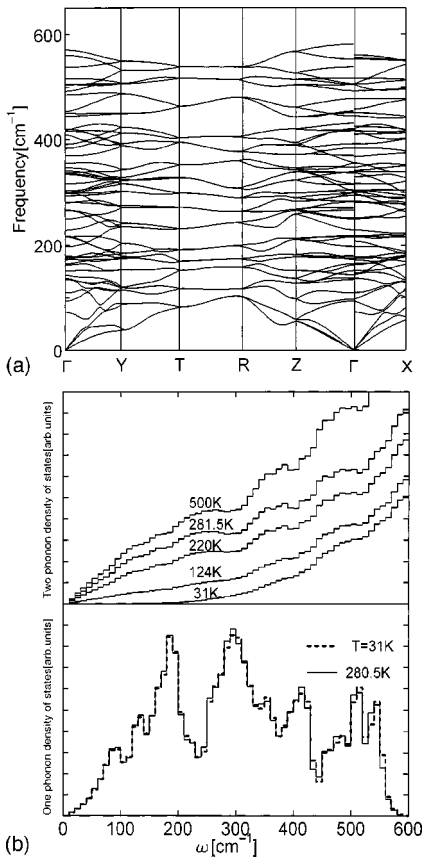

FIG. 4. (a) Phonon-dispersion curves for the $NdGaO_3$ crystal at room temperature. (b) The one- and two-phonon densities of states due to the cubic anharmonic terms at 31 and 280.5 K.

where $n_j(\mathbf{q})=\{\exp[\hbar\omega_j(\mathbf{q})/kT]-1\}^{-1}$ is the phonon occupation number, and $\omega_j(\mathbf{q})$ the temperature-dependent frequency of the normal mode at the wave vector $\mathbf{q}$ and phonon branch j. Especially, Ω is the normal-mode frequency at $\mathbf{q}=0$ and N is the number of unit cells in the crystal.

In the calculations of the one- and two-phonon densities of states due to the cubic anharmonic term, the summations were taken over about 216 wave-vector points in the irreducible first Brillouin zone, therefore, the number of the wave vectors in the first Brillouin zone increases by 1728 points. The δ function was approximated as

$$\delta(x)=\lim_{\varepsilon\to+0}\frac{1}{\pi}\frac{\varepsilon}{x^2+\varepsilon^2}, \tag{5}$$

where ε was taken as 5 cm^{-1}. The one-phonon density of states in 0–600 cm^{-1} of a range at 31 and 280.5 K is shown in Fig. 4(b), where we assumed that thermal-expansion coefficients along *a*, *b*, and *c* were 11.9, 6.6, and 5.8 ($\times10^{-6}$/K),[38,39] respectively. As shown in Fig. 4(b), we found that the one-phonon density of states was approximately independent of temperature in the range between 31 and 280.5 K. The two-phonon density of states in 0 $\sim$600 cm^{-1} in this temperature range is also calculated, assuming the same value of each thermal-expansion coefficient as in the case of the one-phonon density of states. As shown in Figs. 2(a) and 2(b), we found that intensities of two Raman lines [i.e., A_{1g} modes (339 and 470 cm^{-1} at 280.5 K)] were considerably strong in comparison with other ones, and these lines corresponded to 343.8 and 474 cm^{-1} at 31 K, respectively. Thus, we measured two A_{1g} modes (339 and 470 cm^{-1}) in the present study. As shown in Fig. 5, the observed linewidths $\Gamma_j^{(3)}(\omega)$ of A_{1g} modes (339 and 470

TABLE IV. Symmetry vectors of $NdGaO_3$ for *z* direction. These symmetry vectors were driven using the standard projection operator technique. Our calculated phonon eigenvectors are the same as the symmetry vectors and satisfy the orthogonal condition.

Mode	Symmetry vectors $\{x_1,y_1,z_1;\ x_2,y_2,z_2;\ \ldots;\ x_{20},y_{20},z_{20}\}$
A_{1g}	$\{x_1,\ y_1,\ 0;\ -x_1,\ -y_1,\ 0;\ -x_1,\ y_1,\ 0;\ x_1,\ -y_1,\ 0;\ 0,\ 0,\ 0;\ 0,\ 0,\ 0;\ 0,\ 0,\ 0;\ 0,\ 0,\ 0;\ x_9,\ y_9,\ 0;\ -x_9,\ -y_9,\ 0;\ -x_9,\ y_9,\ 0;\ x_9,\ -y_9,\ 0;\ x_{13},\ y_{13},\ z_{13};-x_{13},\ -y_{13},\ -z_{13};\ -x_{13},\ y_{13},\ -z_{13};\ x_{13},\ -y_{13},\ z_{13};\ -x_{13},\ -y_{13},\ z_{13};\ x_{13},\ y_{13},\ -z_{13};\ x_{13},\ -y_{13},\ -z_{13};\ -x_{13},\ y_{13},\ z_{13}\}$
B_{1g}	$\{x_1,\ y_1,\ 0;\ -x_1,\ -y_1,\ 0;\ x_1,\ -y_1,\ 0;\ -x_1,\ y_1,\ 0;\ 0,\ 0,\ 0;\ 0,\ 0,\ 0;\ 0,\ 0,\ 0;\ 0,\ 0,\ 0;\ x_9,\ y_9,\ 0;\ -x_9,\ -y_9,\ 0;\ x_9,\ -y_9,\ 0;\ -x_9,\ y_9,\ 0;\ x_{13},\ y_{13},\ z_{13};-x_{13},\ -y_{13},\ -z_{13};\ x_{13},\ -y_{13},\ z_{13};\ -x_{13},\ y_{13},\ -z_{13};\ -x_{13},\ -y_{13},\ z_{13};\ x_{13},\ y_{13},\ -z_{13};\ -x_{13},\ y_{13},\ z_{13};\ x_{13},\ -y_{13},\ -z_{13}\}$
B_{2g}	$\{0,\ 0,\ z_1;\ 0,\ 0,\ -z_1;\ 0,\ 0,\ -z_1;\ 0,\ 0,\ z_1;\ 0,\ 0,\ 0;\ 0,\ 0,\ 0;\ 0,\ 0,\ 0;\ 0,\ 0,\ 0;\ 0,\ 0,\ z_9;\ 0,\ 0,\ -z_9;\ 0,\ 0,\ -z_9;\ 0,\ 0,\ z_9;\ x_{13},\ y_{13},\ z_{13};\ -x_{13},\ -y_{13},\ -z_{13};\ -x_{13},\ y_{13},\ -z_{13};\ x_{13},\ -y_{13},\ z_{13};\ x_{13},\ y_{13},\ -z_{13};-x_{13},\ -y_{13},\ z_{13};\ -x_{13},\ y_{13},\ z_{13};\ x_{13},\ -y_{13},\ -z_{13}\}$
B_{3g}	$\{0,\ 0,\ z_1;\ 0,\ 0,\ -z_1;\ 0,\ 0,\ z_1;\ 0,\ 0,\ -z_1;\ 0,\ 0,\ 0;\ 0,\ 0,\ 0;\ 0,\ 0,\ 0;\ 0,\ 0,\ 0;\ 0,\ 0,\ z_9;\ 0,\ 0,\ -z_9;\ 0,\ 0,\ z_9;\ 0,\ 0,\ -z_9;\ x_{13},\ y_{13},\ z_{13};-x_{13},\ -y_{13},\ -z_{13};\ x_{13},\ -y_{13},\ z_{13};\ -x_{13},\ y_{13},\ -z_{13};\ x_{13},\ y_{13},\ -z_{13};\ -x_{13},\ -y_{13},\ z_{13};\ x_{13},\ -y_{13},\ -z_{13};\ -x_{13},\ -y_{13},\ z_{13}\}$
A_{1u}	$\{0,\ 0,\ z_1;\ 0,\ 0,\ z_1;\ 0,\ 0,\ -z_1;\ 0,\ 0,\ -z_1;\ x_5,\ y_5,\ z_5;\ -x_5,\ -y_5,\ z_5;\ x_5,\ y_5,\ -z_5;\ -x_5,\ y_5,\ -z_5;\ 0,\ 0,\ z_9;\ 0,\ 0,\ z_9;\ 0,\ 0,\ -z_9;0,\ 0,\ -z_9;\ x_{13},\ y_{13},\ z_{13};\ x_{13},\ y_{13},\ z_{13};\ -x_{13},\ y_{13},\ -z_{13};\ -x_{13},\ y_{13},\ -z_{13};-x_{13},\ -y_{13},\ z_{13};\ -x_{13},\ -y_{13},\ z_{13};\ x_{13},\ -y_{13},\ -z_{13};\ x_{13},\ -y_{13},\ -z_{13}\}$
B_{1u}	$\{0,\ 0,\ z_1;\ 0,\ 0,\ z_1;\ 0,\ 0,\ z_1;\ 0,\ 0,\ z_1;\ x_5,\ y_5,\ z_5;\ -x_5,\ -y_5,\ z_5;\ -x_5,\ y_5,\ z_5;\ x_5,\ -y_5,\ z_5;\ 0,\ 0,\ z_9;\ 0,\ 0,\ z_9;\ 0,\ 0,\ z_9;\ 0,\ 0,\ z_9;\ x_{13},\ y_{13},\ z_{13};\ x_{13},\ y_{13},\ z_{13};\ x_{13},\ -y_{13},\ z_{13};\ x_{13},\ -y_{13},\ z_{13};-x_{13},\ -y_{13},\ z_{13};\ -x_{13},\ -y_{13},\ z_{13};\ -x_{13},\ y_{13},\ z_{13};\ -x_{13},\ y_{13},\ z_{13}\}$
B_{2u}	$\{x_1,\ y_1,\ 0;\ x_1,\ y_1,\ 0;\ -x_1,\ y_1,\ 0;\ -x_1,\ y_1,\ 0;\ x_5,\ y_5,\ z_5;\ x_5,\ y_5,\ -z_5;\ -x_5,\ y_5,\ z_5;\ -x_5,\ y_5,\ -z_5;\ x_9,\ y_9,\ 0;\ x_9,\ y_9,\ 0;\ -x_9,\ y_9,\ 0;\ -x_9,\ y_9,\ 0;\ x_{13},\ y_{13},\ z_{13};\ x_{13},\ y_{13},\ z_{13};\ -x_{13},\ y_{13},\ -z_{13};\ -x_{13},\ y_{13},\ -z_{13};\ x_{13},\ y_{13},\ -z_{13};\ x_{13},\ y_{13},\ -z_{13};\ -x_{13},\ y_{13},\ z_{13};\ -x_{13},\ y_{13},\ z_{13}\}$
B_{3u}	$\{x_1,\ y_1,\ 0;\ x_1,\ y_1,\ 0;\ x_1,\ -y_1,\ 0;\ x_1,\ -y_1,\ 0;\ x_5,\ y_5,\ z_5;\ x_5,\ y_5,\ -z_5;\ x_5,\ -y_5,\ -z_5;\ x_5,\ -y_5,\ z_5;\ x_9,\ y_9,\ 0;\ x_9,\ y_9,\ 0;\ x_9,\ -y_9,\ 0;\ x_9,\ -y_9,\ 0;\ x_{13},\ y_{13},\ z_{13};\ x_{13},\ y_{13},\ z_{13};\ x_{13},\ -y_{13},\ z_{13};\ x_{13},\ -y_{13},\ z_{13};\ x_{13},\ y_{13},\ -z_{13};\ x_{13},\ y_{13},\ -z_{13};\ x_{13},\ -y_{13},\ -z_{13};\ x_{13},\ -y_{13},\ -z_{13}\}$

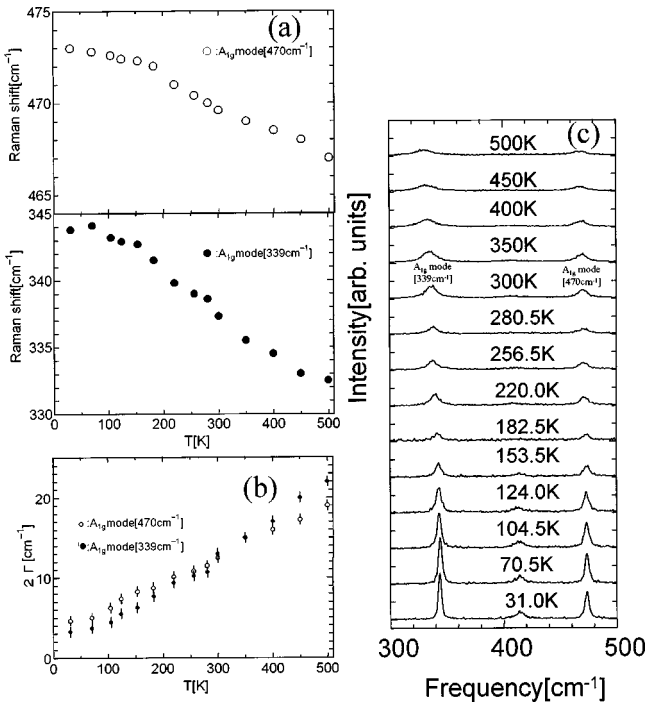

FIG. 5. Temperature dependence of the (a) Raman shift and (b) linewidth for 339- and 470-cm^{-1} peaks of Fig. 2, and (c) Raman spectra of $NdGaO_3$ at different temperatures in the $Z(YY)X$ scattering configuration.

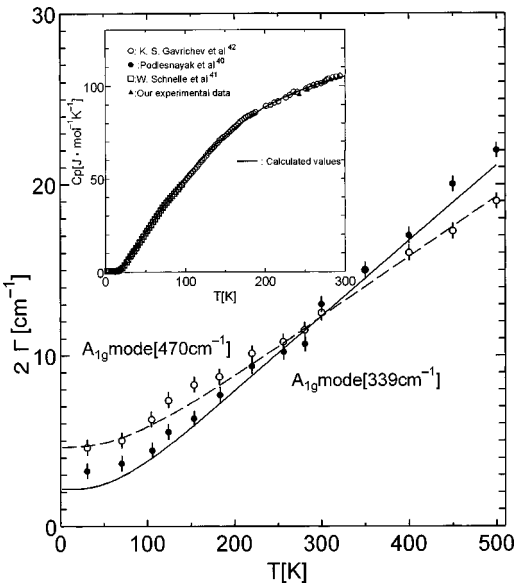

FIG. 6. Temperature dependence of the linewidth of the A_{1g} mode at 339 and 470 cm^{-1}. The observed values at 339 and 470 cm^{-1} are denoted by filed and open circles, respectively, and the calculated ones at 339 and 470 cm^{-1} by the solid and dashed lines, respectively. The inset shows phonon specific-heat capacity *Cp* as a function of temperature. The solid line and filed triangles in the inset were denoted by our calculated and experimental ones, respectively, and the filed circles were analyzed by Podlesnyak *et al.* (Ref. 40) Other symbols (open circles and open squares) were denoted by experimental ones (Refs. 41 and 42).

cm^{-1}) increase monotoneously with the increase of temperature. The accuracy of the experimental linewidths $\Gamma_j^{(3)}(\omega)$ was within about ± 0.3 cm^{-1}. The general cubic anharmonic force coefficient $|C_3|^2$ is analyzed using lattice-dynamical perturbative treatment, which is the same procedure as that used Eqs. (7)–(15) of Ref. 10. The constant $|C_3|^2$ of the A_{1g} (339) and A_{1g} modes (470 cm^{-1}) is obtained as 1.06×10^{10} and 6.38×10^{9} erg^{-1} using Eq. (14) of Ref. 10, where we assumed atomic pairs within 3.0 Å, respectively. As can be seen in Fig. 6, the calculated result for $\Gamma_j^{(3)}(\omega)$ reproduces the observed one in the temperature range of 31–500 K. There seems to be a small disagreement between 2Γ values at the temperature range of 150 K for the A_{1g} mode (470 cm^{-1}) and the calculated one. The reason may be that this discrepancy most likely arises from experimental error at this temperature. However, taking into account the complexity of this class of material and the fact that anharmonicity is calculated on a basis of the lattice-dynamical perturbative treatment, we believe that the overall agreement between theory and experiment should be considered as reasonable. Figure 1(c) shows schematically the measured Raman mode of A_{1g} symmetry using the symmetry vectors in Table IV. These assignments are reasonable with those in comparison to $RMnO_3$ (R=Y and La).[43] Therefore, A_{1g} (339) and A_{1g} modes (470 cm^{-1}) can be considered as pure modes in a good approximation because modes involving motions of mainly R atoms have frequencies following roughly the $m_R^{-1/2}$ dependence.[43] The peak of the A_{1g} mode (470 cm^{-1}) corresponds to a phase stretching mode of the oxygen cage. The peak of the A_{1g} mode (339 cm^{-1}) is attributed to an out-of-phase x rotation of the oxygen as a librational mode. Therefore, the A_{1g} mode (339 cm^{-1}) does not involve internal distortions of the GaO_6 octahedra. Therefore, the linewidths for the A_{1g} mode (339 cm^{-1}) varied with increasing temperature by comparison with those of the A_{1g} mode (470 cm^{-1}). As previously reported,[9] several oxide crystals (with a high melting point and stable structure in high-temperature ranges) usually tend to have small values of $|C_3|^2$ in the range of 10^9-10^{11} erg^{-1}. Therefore, the present values of $|C_3|^2$ indicate that the $NdGaO_3$ crystal has the characteristic of a stable structure in high-temperature ranges. From this fact, it is concluded that the temperature dependence of the linewidth of A_{1g} modes for the $NdGaO_3$ crystal can be explained approximately considering the cubic anharmonic term in the expansion series of the crystal potential energy. By using this temperature-dependent one-phonon density of states, the temperature dependence of the molar specific-heat capacity *Cp* is also calculated, as shown in the inset of Fig. 6, where we found that our calculated values agree with results of calculated values[40] and experimental values[41,42] in the temperature range between 2.24 and 300 K. Furthermore, we have calculated the heat capacity and have compared the calculated values with experimental ones by using the rigid-ion model for several other crystal structures.[4,5,7,8] The calculated results agree with the experimental values at both low- and high-temperature regions in those cases.

IV. CONCLUSION

The Raman- and infrared-active phonon frequencies of the $NdGaO_3$ crystal have been experimentally determined at room temperature. The phonon-dispersion curves of the $NdGaO_3$ crystal are calculated on the basis of a rigid-ion model using the measured frequency values, and the average deviation between calculated and experimental values at the 1 point is approximately 14.8 cm^{-1}. The temperature dependence of the Raman linewidth of the A_{1g} modes (339 and 470 cm^{-1}) is analyzed by the temperature-dependent two-phonon density of states due to the cubic anharmonic term. The values of $|C_3|^2$ for $\Gamma_j^{(3)}(\omega)$ are analyzed using calculated phonon dispersions based on lattice-dynamical perturbative treatment. The calculated linewidths for the A_{1g} mode reproduce the observed one in the temperature range between 31 and 500 K. The phonon specific heat Cp was analyzed by the calculated one-phonon density of states and agrees with experimental values in the temperature range between 2.24 and 300 K. From this fact it is concluded that the temperature dependence of the linewidth of the $NdGaO_3$ crystal is approximately explained by the cubic anharmonic term in the expansion series of the crystal potential energy. Therefore this indicates that the present model is useful to drive the lattice-dynamical properties.

ACKNOWLEDGMENTS

We greatly thank Professor S. Onari of Tsukuba University for permitting the use of the FT-IR spectrometer. We also heartily thank S. Kiyomoto of Tsukuba University for technical assistance.

*Email address: suda@aomori-pc.ac.jp

†Present address: Department of Computational Science, Faculty of Science, Kanazawa University, Kanazawa 920-11.

[1] H. Bilz and W. Kress, *Phonon Dispersion Relations in Insulators*, edited by M. Cardona, P. Fulde, and H.-J. Queisser, Springer Series in Solid-State Science Vol. 10 (Springer-Verlag, Heidelberg, 1979).

[2] T. Sato and T. Asari, J. Phys. Soc. Jpn. **64**, 1193 (1995).

[3] N. Kimura and T. Sato, J. Phys. Soc. Jpn. **63**, 3704 (1994).

[4] T. Sato and J. Suda, J. Phys. Soc. Jpn. **67**, 3809 (1998).

[5] T. Sato and J. Suda, J. Phys. Soc. Jpn. **65**, 482 (1996).

[6] J. Suda and T. Sato, J. Spectrosc. Soc. Jpn. **46**, 238 (1997).

[7] J. Suda, T. Itoh, and T. Sato, J. Spectrosc. Soc. Jpn. **48**, 179 (1999).

[8] J. Suda and T. Sato, J. Phys. Soc. Jpn. **66**, 1707 (1997).

[9] J. Suda, H. Chiba, and T. Sato, J. Phys. Soc. Jpn. **67**, 20 (1998).

[10] T. Shinagawa, J. Suda, T. Sato, and H. Saito, J. Phys. Soc. Jpn. **69**, 465 (2000).

[11] M. I. Filk, Z. M. Zhang, K. E. Goodson, M. P. Siegal, and J. M. Phillips, Phys. Rev. B **46**, 5606 (1992).

[12] Z. M. Zhang and M. I. Filk, IEEE Trans. Appl. Supercond. **3**, 1604 (1993).

[13] C. G. Malone, Z. M. Zhang, M. I. Filk, and E. G. Cravalho, IEEE Trans. Appl. Supercond. **3**, 2852 (1993).

[14] J. R. Jasperse, A. Kahn, J. N. Plendle, and S. S. Mitra, Phys. Rev. **146**, 256 (1966).

[15] W. G. Spitzer, R. C. Miller, D. A. Kleinman, and L. E. Howarth, Phys. Rev. **126**, 1710 (1962).

[16] A. S. Barker, Jr. and M. Tinkham, Phys. Rev. **125**, 1527 (1962).

[17] J. C. Galzerrani and R. S. Katiyar, Solid State Commun. **41**, 515 (1982).

[18] R. L. Sandstrom, E. A. Giess, W. J. Gallagher, A. Segmuller, E. I. Cooper, M. F. Chisholm, A. Guptas, S. Shinde, and R. B. Laibowitz, Appl. Phys. Lett. **53**, 1874 (1988).

[19] G. Koren, A. Gupta, E. A. Giess, A. Segmuller, and R. B. Laibowitz, Appl. Phys. Lett. **54**, 1054 (1989).

[20] M. Marezio, J. P. Remeika, and P. D. Dernier, Inorg. Chem. **7**, 1337 (1968).

[21] E. C. Prado, A. R. Figueroa, and R. S. Katiyar, J. Appl. Phys. **78**, 1920 (1995).

[22] L. Sun, Y. F. Chen, C. Z. Ge, T. Yu, M. S. Zhang, N. B. Ming, D. S. Ding, and Y. Chang, Phys. Rev. B **55**, 12 218 (1997).

[23] L. Sun, Y. F. Chen, C. Z. Ge, T. Yu, M. S. Zhang, N. B. Ming, D. S. Ding, and Y. Chang, Z. Phys. B: Condens. Matter **102**, 479 (1997).

[24] P. Calvani, M. Capizzi, F. Donato, P. Dore, S. Lupi, P. Maselli, and C. P. Varsamis, Physica C **181**, 289 (1991).

[25] Z. M. Zhang, B. I. Choi, M. I. Flik, and A. C. Anderson, J. Opt. Soc. Am. B **11**, 2252 (1994).

[26] R. Buhleier, S. D. Bronson, I. E. Trofimov, J. O. White, H. U. Habermeier, and J. Kuhl, Phys. Rev. B **50**, 9672 (1994).

[27] C. Ludwig, J. Kuhl, and J. O. White, J. Opt. Commun. **41**, 515 (1982).

[28] M. L. Sanjuan, V. M. Orera, R. I. Merino, and J. Blasco, J. Phys.: Condens. Matter **10**, 11 687 (1998).

[29] H. Saito, Master's thesis, Hirosaki University, 1999.

[30] R. W. G. Wychoff, *Crystal Structure* (Krieger, Malabar, Florida, 1986).

[31] O. Kamishima, H. Koyama, R. Takashashi, Y. Abe, T. Sato, and H. Hattori, J. Phys.: Condens. Matter **14**, 3905 (2002).

[32] R. F. Wallis, I. P. Ipatova, and A. A. Maradudin, Fiz. Tverd. Tela (St. Petersburg) **8**, 10 (1996) [Sov. Phys. Solid State **8**, 850 (1966)].

[33] E. Idarokapis, E. Anastassakis, and G. A. Kouroukils, Phys. Rev. B **32**, 8346 (1985).

[34] I. P. Ipatova, A. A. Maradudin, and R. F. Wallis, Phys. Rev. **155**, 882 (1967).

[35] M. R. Monga, V. K. Jindal, and K. N. Pathak, Phys. Rev. B **19**, 1230 (1979).

[36] M. Balkanski, R. F. Wallis, and H. Haro, Phys. Rev. B **28**, 1928 (1983).

[37] K. Nishidate, K. Nishikawa, M. Suhara, and T. Sato, J. Phys.: Condens. Matter **5**, 4855 (1993).

[38] M. Sasaura, S. Miyazawa, and M. Mukaida, J. Appl. Phys. **68**, 3643 (1990).

[39] W. Marti, P. Fisher, F. Altorfer, H. J. Scheel, and M. Tadin, J. Phys.: Condens. Matter **6**, 127 (1994).

[40] A. Podlesnayak, S. Rosenkranz, F. Fauth, W. Marti, A. Furrer, A. Mirmelstein, and H. J. Scheel, J. Phys.: Condens. Matter **5**, 8987 (1993).

[41] W. Schnelle, R. Fischer, and E. Gmelin, J. Phys. D **34**, 846 (2001).
[42] K. S. Gavichev, V. E. Gorbunov, L. N. Golushina, G. A. Totorova, E. A. Tishchenko, Y. G. Nadtochii, and Y. B. Poyarkov, Inorg. Mater. (Transl. of Neorg. Mater.) **30**, 1346 (1994).
[43] M. N. Iliev, M. V. Abrashev, H.-G. Lee, V. N. Popov, Y. Y. Sun, C. Thomsen, R. L. Meng, and C. W. Chu, Phys. Rev. B **57**, 2872 (1998).